PHYSICAL REVIEW D **91,** 115014 (2015)

# Angular asymmetries as a probe for anomalous contributions to *HZZ* vertex at the LHC

N. Belyaev

*National Research Nuclear University (Moscow Engineering Physics Institute), 31 Kashirskoe Shosse, Moscow 115409, Russia*

R. Konoplich*

*Department of Physics, New York University, 4 Washington Place, New York, New York 10003, USA*

L. Egholm Pedersen

*Niels Bohr Institute, University of Copenhagen, Blegdamsvej 17 Kobenhavn 2100, Denmark*

K. Prokofiev†

*Department of Physics, Hong Kong University of Science and Technology, Clear Water Bay, Kowloon, Hong Kong*

(Received 18 February 2015; published 15 June 2015)

In this article, the prospects for studying the tensor structure of the $HZZ$ vertex with the LHC experiments are presented. The structure of tensor couplings in Higgs di-boson decays is investigated by measuring the asymmetries and by studying the shapes of the final state angular distributions. The expected background contributions, detector resolution, and trigger and selection efficiencies are taken into account. The potential of the LHC experiments to discover sizeable non-Standard Model contributions to the $HZZ$ vertex with 300 and 3000 $\mathrm{fb}^{-1}$ is demonstrated.

DOI: 10.1103/PhysRevD.91.115014 PACS numbers: 12.60.Fr, 14.80.Ec

## I. INTRODUCTION

In the summer of 2012, the CMS and ATLAS Collaborations at the LHC reported the discovery of a new neutral resonance in searches for the Standard Model Higgs boson. This discovery was later confirmed by analyses of the full LHC Run-I data set by both collaborations [1,2]. It was demonstrated that the new particle with a mass around 125.5 GeV was dominantly produced via the gluon fusion process and decays into pairs of gauge bosons: $\gamma\gamma$, $ZZ$ and $WW$. The observed production and decay modes identified the discovered particle as a neutral boson. The subsequent measurement of its couplings to fermions and bosons demonstrated the compatibility of the discovered resonance with the expectations for the Standard Model Higgs boson within available statistics [3–5].

In the Standard Model, electroweak symmetry breaking via the Higgs mechanism requires the presence of a single neutral Higgs boson with spin 0 and even $CP$ parity. Theories beyond the Standard Model often require an extended Higgs sector featuring several neutral Higgs bosons of both even- and odd-$CP$ parity. In such a case, mixing between Higgs boson $CP$ eigenstates is possible. The Higgs boson mass eigenstates observed in experiment may, thus, have mixed $CP$ parity. Such an extension of the Higgs sector is important because effects of $CP$ violation in the SM are too small and, in particular, cannot explain the baryon asymmetry of the Universe.

Dedicated studies of spin and parity of the Higgs candidate discovered by ATLAS and CMS showed that its dominant spin and parity are compatible with $J^{CP} = 0^{++}$ [4–6]. The data set of about 25 $\mathrm{fb}^{-1}$ currently collected by each of the major LHC experiments allows us to set an upper limit on the possible $CP$-odd contribution. The sensitivity is expected to improve with larger data sets to be collected at the LHC.

There have been many works on direct measurement of $CP$ violation in the Higgs sector [7–32]. In this paper the sensitivity of LHC experiments to observe $CP$-mixing effects with 300 and 3000 $\mathrm{fb}^{-1}$ is evaluated using the method of angular asymmetries.

This paper is organized as follows. In Sec. II observables sensitive to $CP$ violation in the $HZZ$ vertex are discussed. The spin-0 model, a Monte Carlo production of signal and background, and a Lagrangian parametrization for $CP$-mixing measurements are discussed in Sec. III. In Sec. IV the expected sensitivity of the LHC experiments to the $CP$-violation effects based on angular asymmetries is presented. Constraits are set on the contribution of anomalous couplings to the $HZZ$ vertex. Section V introduces the measurement technique based on observables fit. Exclusion

*Also at Physics Department, Manhattan College, 4513 Manhattan College Parkway, Riverdale, New York, New York 10471, USA.

†Also at Institute for Advanced Study, HKUST, Clear Water Bay, Kowloon, Hong Kong.

 

regions for the mixing angle are presented. Section VI gives the overall summary of obtained results.

## II. OBSERVABLES

In this paper we study the sensitivity of final state observables to the $CP$ violating $HZZ$ vertex in the process:

$$gg \to H \to ZZ \to 4l. \tag{1}$$

Following the notation introduced in [21], the general scattering amplitude describing interactions of a spin-zero boson with the gauge bosons is given by

$$A(X \to VV) = \frac{1}{v}\left(g_1 m_V^2 \epsilon_1^* \epsilon_2^* + g_2 f_{\mu\nu}^{*(1)} f^{*(2)\mu\nu} + g_4 f_{\mu\nu}^{*(1)} \tilde{f}^{*(2)\mu\nu}\right). \tag{2}$$

Here the $f^{(i)\mu\nu} = \epsilon_i^\mu q_i^\nu - \epsilon_i^\nu q_i^\mu$ is the field strength tensor of a gauge boson with momentum $q_i$ and polarization vector $\epsilon_i$; $\tilde{f}^{(i)\mu\nu} = 1/2\epsilon^{\mu\nu\alpha\beta} f_{\alpha\beta}$ is the conjugate field strength tensor. The symbols $v$ and $m_V$ denote the SM vacuum expectation value of the Higgs field and the mass of the gauge boson, respectively.

In the Standard Model, the only nonvanishing coupling of the Higgs to $ZZ$ or $WW$ boson pairs at tree-level is $g_1 = 2i$, while $g_2$ is generated through radiative corrections. For final states with at least one massless gauge boson, such as $\gamma\gamma$, $gg$ or $Z\gamma$, the SM interactions with the Higgs boson are loop-induced. These interactions are described by the coupling $g_2$. The coupling $g_4$ is associated with the interaction of $CP$-odd Higgs boson with a pair of gauge bosons. The simultaneous presence of $CP$-even terms $g_1$ and/or $g_2$ and the $CP$-odd term $g_4$ leads to $CP$ violation.

In general, $g_i$ couplings can be complex and momentum dependent. However imaginary parts of these couplings are generated by absorptive parts of the corresponding diagrams and expected to be small: approximately less than 1%. We further assume that the energy scale of new physics is around 1 TeV or higher, so that the momentum dependence of the couplings can be neglected. Thus, in the following we will consider $g_i$ couplings as real and momentum-independent.

These assumptions are entirely consistent with the framework of an effective field theory (EFT) of the SM. If the energy scale of the new physics is much higher than the electroweak scale new effects can be described by an EFT with the SM Lagrangian supplemented by higher dimension operators of $d = 6$. Such an approach was worked out in detail in [33,34].

One of possibilities to study $CP$ violation in the process of Eq. (1) is to analyze the shapes of angular and mass distributions of the final state [35,36]. The common choice of angular observables for this type of analysis is show in Fig. 1.

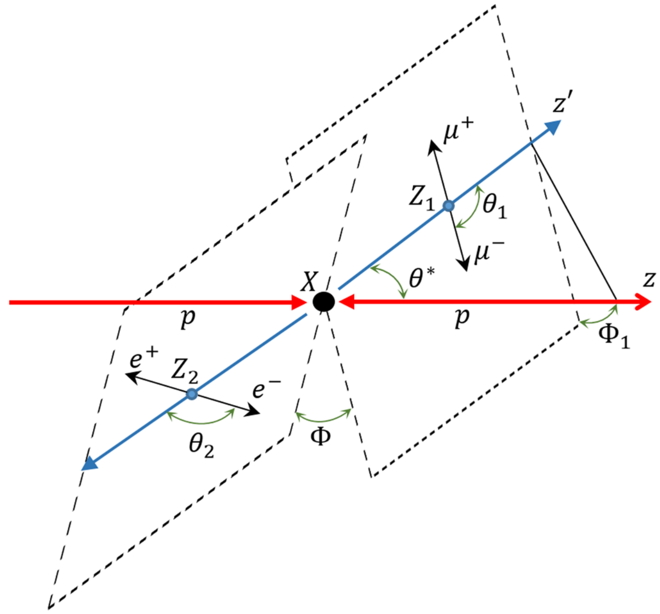


FIG. 1 (color online). Definitions of the $CP$-sensitive final state angular observables in $gg \to H \to ZZ \to 4l$ decay.

A complimentary approach is based on studies of angular-function asymmetries arising in the case of $CP$ violation. There are six observable functions proposed in [16]. The first angular observable function is defined as follows:

$$O_1 = \frac{(\vec{p}_{2Z} - \vec{p}_{1Z}) \cdot (\vec{p}_{3H} + \vec{p}_{4H})}{|\vec{p}_{2Z} - \vec{p}_{1Z}||\vec{p}_{3H} + \vec{p}_{4H}|}.$$

Here $\vec{p}_i$, $i = 1, \ldots 4$ are the 3-momenta of the final state leptons in the order $l_1 \bar{l}_1 l_2 \bar{l}_2$. The subscripts $Z$ and $H$ denote that the corresponding 3-vector is taken in the $Z$ or in the Higgs boson rest frames. Using these definitions, the second observable function reads

$$O_2 = \frac{(\vec{p}_{2Z} - \vec{p}_{1Z}) \cdot (\vec{p}_{4H} \times \vec{p}_{3H})}{|\vec{p}_{2Z} - \vec{p}_{1Z}||\vec{p}_{4H} \times \vec{p}_{3H}|}.$$

The third observable function $O_3$ is constructed using $O_1$,

$$O_3 = O_1 O_{3a} O_{3b},$$

where

$$O_{3a} = \frac{(\vec{p}_{4Z} - \vec{p}_{3Z}) \cdot (\vec{p}_{1H} \times \vec{p}_{2H})}{|\vec{p}_{4Z} - \vec{p}_{3Z}||\vec{p}_{1H} \times \vec{p}_{2H}|}$$

and

$$O_{3b} = \frac{(\vec{p}_{3Z} - \vec{p}_{4Z}) \cdot (\vec{p}_{1H} + \vec{p}_{2H})}{|\vec{p}_{3Z} - \vec{p}_{4Z}||\vec{p}_{1H} + \vec{p}_{2H}|}.$$

The remaining three observable functions are given by

$$O_4 = \frac{[(\vec{p}_{3H}\times\vec{p}_{4H})\cdot\vec{p}_{1H}][(\vec{p}_{3H}\times\vec{p}_{4H})\cdot(\vec{p}_{1H}\times\vec{p}_{2H})]}{|\vec{p}_{3H}+\vec{p}_{4H}|^2|\vec{p}_{1H}+\vec{p}_{2H}||\vec{p}_{3Z}-\vec{p}_{4Z}|^2|\vec{p}_{1Z}-\vec{p}_{2Z}|^2/16},$$

$$O_5 = \frac{[(\vec{p}_{4H}\times\vec{p}_{3H})\cdot\vec{p}_{1H}][(\vec{p}_{1Z}-\vec{p}_{2Z})\cdot\vec{p}_{3Z}]}{|\vec{p}_{3H}+\vec{p}_{4H}||\vec{p}_{3Z}-\vec{p}_{4Z}|^2|\vec{p}_{1Z}-\vec{p}_{2Z}|^2/8},$$

and

$$O_6 = \frac{[(\vec{p}_{1Z}-\vec{p}_{2Z})\cdot(\vec{p}_{3H}+\vec{p}_{4H})][(\vec{p}_{3H}\times\vec{p}_{4H})\cdot\vec{p}_{1H}]}{|\vec{p}_{1Z}-\vec{p}_{2Z}|^2|\vec{p}_{3H}+\vec{p}_{4H}|^2|\vec{p}_{3Z}-\vec{p}_{4Z}|/4}.$$

These observables are related to the final state angular variables defined in [35] and illustrated in Fig. 1. For instance, a trivial calculation yeilds $O_1=\cos\theta_1$ and $O_2=-\sin\phi\sin\theta_1$.

Note that the total cross section is $CP$ even (no interference between $CP$-even and $CP$-odd terms) and cannot be used to detect the presence of $CP$-violating terms in the $HZZ$ vertex.

## III. SPIN-0 MODEL AND MONTE CARLO PRODUCTION

The dominant Higgs boson production mechanism at the LHC is gluon fusion. To simulate the production of a Higgs-like boson and its consequent decay into $ZZ$ and $4l$, the MadGraph5 Monte Carlo generator [37] was used. This generator implements the Higgs Characterization model [38]. The corresponding effective Lagrangian describing the interaction of the spin-0 Higgs-like boson with vector bosons is given by

$$\begin{aligned}\mathcal{L}_0^V = \Bigg\{ & c_\alpha\kappa_{\rm SM}\left[\frac{1}{2}g_{\rm HZZ}Z_\mu Z^\mu + g_{\rm HWW}W_\mu^+W^{-\mu}\right] - \frac{1}{4}[c_\alpha\kappa_{H\gamma\gamma}g_{H\gamma\gamma}A_{\mu\nu}A^{\mu\nu} + s_\alpha\kappa_{A\gamma\gamma}g_{A\gamma\gamma}A_{\mu\nu}\tilde{A}^{\mu\nu}] \\ & -\frac{1}{2}[c_\alpha\kappa_{HZ\gamma}g_{HZ\gamma}Z_{\mu\nu}A^{\mu\nu} + s_\alpha\kappa_{AZ\gamma}g_{AZ\gamma}Z_{\mu\nu}\tilde{A}^{\mu\nu}] - \frac{1}{4}[c_\alpha\kappa_{Hgg}g_{Hgg}G^a_{\mu\nu}G^{a,\mu\nu} + s_\alpha\kappa_{Agg}g_{Agg}G^a_{\mu\nu}\tilde{G}^{a,\mu\nu}] \\ & -\frac{1}{4}\frac{1}{\Lambda}[c_\alpha\kappa_{HZZ}Z_{\mu\nu}Z^{\mu\nu} + s_\alpha\kappa_{AZZ}Z_{\mu\nu}\tilde{Z}^{\mu\nu}] - \frac{1}{2}\frac{1}{\Lambda}[c_\alpha\kappa_{HWW}W^+_{\mu\nu}W^{-\mu\nu} + s_\alpha\kappa_{\rm AWW}W^+_{\mu\nu}\tilde{W}^{-\mu\nu}] \\ & -\frac{1}{\Lambda}c_\alpha[\kappa_{H\partial\gamma}Z_\nu\partial_\mu A^{\mu\nu} + \kappa_{H\partial Z}Z_\nu\partial_\mu Z^{\mu\nu} + (\kappa_{H\partial W}W_\nu^+\partial_\mu W^{-\mu\nu} + {\rm H.c.})]\Bigg\}X, \end{aligned} \tag{3}$$

where $\Lambda$ is the new physics energy scale and the field strength tensors are defined as follows:

$$V_{\mu\nu} = \partial_\mu V_\nu - \partial_\nu V_\mu \quad (V = A, Z, W^\pm),$$
$$G^a_{\mu\nu} = \partial_\mu G^a_\nu - \partial_\nu G^a_\mu + g_s f^{abc}G^b_\mu G^c_\nu.$$

The dual tensor $\tilde{V}_{\mu\nu}$ is defined as

$$\tilde{V}_{\mu\nu} = \frac{1}{2}\epsilon_{\mu\nu\rho\sigma}V^{\rho\sigma}.$$

The mixing angle $\alpha$ allows the production and decay of $CP$-mixed states and implies $CP$ violation when $\alpha \neq 0$ or $\alpha \neq \pi/2$. The definitions of effective tensor couplings $g_{XVV'}$ are shown in Table I.

The Lagrangian in Eq. (3) is an effective Lagrangian with $U(1)_{\rm EM}$ symmetry. It parametrizes all possible Lorentz structures, is not $SU(2)\times U(1)$ invariant and does not assume that the Higgs boson belongs to a doublet of the weak $SU(2)$ group. Interaction terms corresponding to a Lagrangian of this type do not necessarily form a complete basis. However, this form is convenient for analysis of experimental data, as it relates in a simple way effective couplings and quantities observed in experiments. Note that there is a different and very popular EFT approach [34] to

TABLE I. Definitions of effective tensor couplings $g_{XVV'}$ introduced in Eq. (3) in units of the Higgs vacuum expectation $v$. The symbol $C$ is defined as: $C = \sqrt{\frac{\alpha_{\rm EM}G_F m_Z^2}{8\sqrt{2}\pi}}$.

| | $ZZ/WW$ | $\gamma\gamma$ | $Z\gamma$ | $gg$ |
|---|---|---|---|---|
| $v\cdot g_{HVV'}$ | $2m^2_{Z/W}$ | $\frac{47\alpha_{\rm EM}}{18\pi}$ | $C\frac{94\cos^2\theta_W-13}{9\pi}$ | $-\frac{\alpha_s}{3\pi}$ |
| $v\cdot g_{AVV'}$ | 0 | $\frac{4\alpha_{\rm EM}}{3\pi}$ | $2C\frac{8\cos^2\theta_W-5}{3\pi}$ | $\frac{\alpha_s}{2\pi}$ |

TABLE II. Conversion coefficients between parameters of the Lagrangian of Eq. (3) and tensor couplings of the effective amplitude of Eq. (2).

| Coupling | ZZ | WW | $\gamma\gamma$ | $Z\gamma$ | $gg$ |
|---|---|---|---|---|---|
| $g_1/2ic_a$ | $k_{\rm SM}$ | $k_{\rm SM}$ | $\cdots$ | $\cdots$ | $\cdots$ |
| $g_2/2ic_a$ | $\tilde{K}_{HZZ}$ | $\tilde{K}_{HWW}$ | $\tilde{K}_{H\gamma\gamma}$ | $\tilde{K}_{HZ\gamma}$ | $\tilde{K}_{Hgg}$ |
| $g_4/2is_a$ | $\tilde{K}_{AZZ}$ | $\tilde{K}_{AWW}$ | $\tilde{K}_{A\gamma\gamma}$ | $\tilde{K}_{AZ\gamma}$ | $\tilde{K}_{Agg}$ |
| $g_1'/2ic_a$ | $\tilde{K}_{H\partial Z}$ | $\mathrm{Re}(\tilde{K}_{H\partial W})$ | $\cdots$ | $\cdots$ | $\cdots$ |
| $g_1'''/2ic_a$ | $\cdots$ | $i\mathrm{Im}(\tilde{K}_{H\partial W})$ | $\cdots$ | $\cdots$ | $\cdots$ |

studies of the Higgs boson sector based on a complete set of operators of dimension six (the so-called Warsaw basis).

The relations between parameters of the Lagrangian of Eq. (3) and tensor couplings of the effective amplitude of Eq. (2) can be derived from Feynman rules. The corresponding conversion coefficients are shown in Table II.

In this table the following definitions are used:

$$\tilde{K}_{XVV'} = \frac{1}{4}\frac{v}{\Lambda}\tilde{g}_{XVV'}k_{XVV'},$$

$$\tilde{K}_{H\partial V} = \frac{1}{2}\frac{v}{\Lambda}\left(\frac{\Lambda_1}{m_V}\right)^2 k_{H\partial V},$$

$$c_\alpha = \cos\alpha, \quad \text{and} \quad s_\alpha = \sin\alpha.$$

Here $X$ denotes either $H$ or $A$ and the index $VV'$ denotes the final state gauge boson pair. The effective couplings $\tilde{g}_{XVV'}$ are defined as follows:

(i) In the case of $ZZ$ or $WW$ interactions, $\tilde{g}_{XVV'} = 1$;

(ii) For $\gamma\gamma$, $Z\gamma$ and $gg$ interactions, couplings $\tilde{g}_{XVV'}$ are equivalent to the couplings $g_{XVV'}$ defined in Table I.

The couplings $\tilde{K}_{H\partial V}$, where $V = W, Z, \gamma$, correspond to the so-called contact terms of the Higgs Characterization Lagrangian of Eq. (3). These contact terms can be reproduced in the amplitude of Eq. (2) by reparametrizing the $g_1$ coupling in the following form [39]:

$$g_1(q_1^2, q_2^2) = g_1^{SM} + g_1^2\frac{|q_1^2| + |q_2^2|}{\Lambda_1^2} + g_1^3\frac{|q_1^2| - |q_2^2|}{\Lambda_1^2}.$$

This equation represents the leading terms of the form factor expansion. In the case of complex $k_{H\partial W}$, the momenta of the $W$ bosons should be assigned as follows: $q_1$ for $W^-$ and $q_2$ for $W^+$. In the case of $HZ\gamma$ interaction with a real photon, the term proportional to $k_{H\partial\gamma}$ vanishes.

In the following we will consider a model based on the Lagrangian of Eq. (3) in which the mixing is provided by the simultaneous presence of the Standard model $CP$-even term and a non-Standard Model $CP$-odd term in the $HZZ$ decay vertex. The signal Monte Carlo samples used in this analysis are produced using the Higgs Characterization model parameters presented in Table III.

TABLE III. Parameters of Higgs Characterization model used for Monte Carlo simulation of signal samples.

| $k_{SM}$ | $k_{HZZ}$ | $k_{AZZ}$ | $k_{Hgg}$ | $k_{Agg}$ | $\Lambda$, GeV |
|---|---|---|---|---|---|
| 1 | 0 | 28.6 | 1 | 1 | $10^3$ |

The coefficient $k_{\rm AZZ}$ was chosen such that it provided equal cross sections for decays of $CP$-odd and $CP$-even Higgs states: $\sigma(c_\alpha = 0) = \sigma(c_\alpha = 1)$. The tensor couplings for the decay vertex corresponding to the amplitude of Eq. (2) can be restored using the following relations: $g_2 = 2ic_\alpha$ and $g_4 = 2is_\alpha\tilde{K}_{AZZ}$, where $\tilde{K}_{AZZ} = 1.76$. It is noted that the factor $2i$ is not important in the study of asymmetries because it defines the overall cross section normalization.

The signal samples were produced using the MadGraph5 Monte Carlo generator [37]. These samples were created in the range of mixing angles $-1 \le \cos\alpha \le 1$ in steps of 0.05. The dominant background processes $q\bar{q} \to ZZ, Z\gamma$ were also simulated with MadGraph5.

After simulation of signal and background events at $\sqrt{s} = 14$ TeV, the parton showering was performed using the PYTHIA6 Monte Carlo generator [40]. Generic detector effects were included by using the PGS package [37]. The main detector parameters used for this simulation are presented in Table IV. For comparison, the expected acceptance, efficiencies and resolutions of the ATLAS and CMS detectors of the LHC can be found in [41,42]. Finally a kinematic selection was applied. It was required that candidates decayed to two same flavor oppositely charged lepton pairs. If several of such candidates could be reconstructed in an event, the leptons pairs with invariant masses closest to the on-shell Z mass where chosen. Each individual lepton had a pseudorapidity $|\eta| < 2.5$ and transverse momentum $p_T > 7$ GeV. The most energetic lepton should satisfy $p_T > 20$ GeV whereas the second (third) similarly had $p_T > 15$ GeV ($p_T > 10$ GeV). The invariant mass of the on-shell $Z$ boson was in the mass window (50,106) GeV while the off-shell $Z$ boson $m_{Z*} > 20$ GeV. Only Higgs candidates in the signal region 115 GeV $< m_H <$ 130 GeV where

TABLE IV. Tuning parameters used to simulate detector effects with PGS package.

| Parameter | Value |
|---|---|
| Electromagnetic calorimeter resolution $\cdot\sqrt{E}$ | 0.1 |
| Hadronic calolrimeter resolution$\cdot\sqrt{E}$ | 0.8 |
| MET resolution | 0.2 |
| Outer radius of tracker (m) | 1.0 |
| Magnetic field (T) | 2.0 |
| Track finding efficiency | 0.98 |
| Tracking $\eta$ coverage | 2.5 |
| $e/\gamma\eta$ coverage | 2.8 |
| Muon $\eta$ coverage | 2.8 |

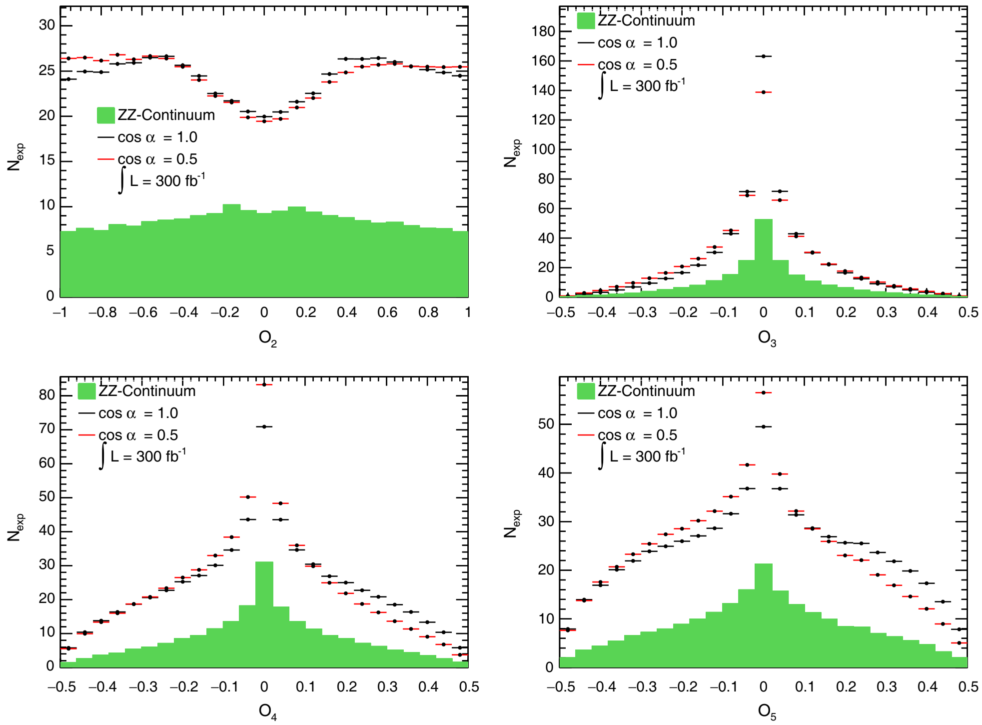


FIG. 2 (color online). Distributions of observables $O_2, O_3, O_4$ and $O_5$ for two values of the mixing angle $\alpha$.

considered. The selection is a simplified version of the one presented in [2].

## IV. ASYMMETRIES

For each observable $O_i$ sensitive to $CP$ violation, the corresponding asymmetry can be defined as

$$A_i = \frac{N(O_i > 0) - N(O_i < 0)}{N(O_i > 0) + N(O_i < 0)}, \tag{4}$$

where $N$ is the number of events with the observable less or greater than zero. Integrating the corresponding decay probabilities, it can be shown that these asymmetries directly probe the tensor couplings defined in the amplitude of Eq. (2) [16]. The value of $A_1$ is proportional to $\mathrm{Im}(g_4)$, while $A_2, A_3, A_4, A_5$ and $A_6$ probe the values of $\mathrm{Re}(g_4)$ and $\mathrm{Im}(g_2)$, respectively.

Analysis of asymmetries sensitive to $CP$ violation for the process of Eq. (1) was performed in [16]. In this section we extend this analysis by including effects of parton showering, hadronization, generic detector effects and contributions from the irreducible $q\bar{q} \to ZZ/Z\gamma \to 4l$ background. Lepton interference in the final state and the contribution of two off-shell $Z$ bosons are also taken into account.

The distributions of observables $O_2, O_3, O_4$ and $O_5$ for two values of the mixing angle $\cos\alpha = 1$ and $\cos\alpha = 0.5$ are shown in Fig. 2. Signal $H \to ZZ \to 4l$ events are generated using the production and decay model defined in Table III. The contributions from the signal and $q\bar{q} \to ZZ \to 4l$ background are normalized to their respective expectations at 300 $\mathrm{fb}^{-1}$. It is noted that the presence of $CP$-mixing leads to distortions of distributions of selected observables. The distributions of $O_2$ through $O_5$ become asymmetric in the presence of a real component of $g_4$. This asymmetry is especially pronounced for $O_4$ and $O_5$. As suggested in [16], the background is $CP$ conserving and the corresponding distributions of observables are symmetric. The shapes of asymmetries $A_i$ for the model presented in Table III are shown in Fig. 3. The pure $CP$-even and $CP$-odd cases are given by $\cos\alpha = 1$ and $\cos\alpha = 0$, respectively.

Note, that according to the structure of Lagrangian [Eq. (3)] the $CP$-violating contribution is defined by the parameter $p = \tilde{K}_{AZZ} \tan\alpha$. This parameter, thus, determines the corresponding asymmetries of angular observables.

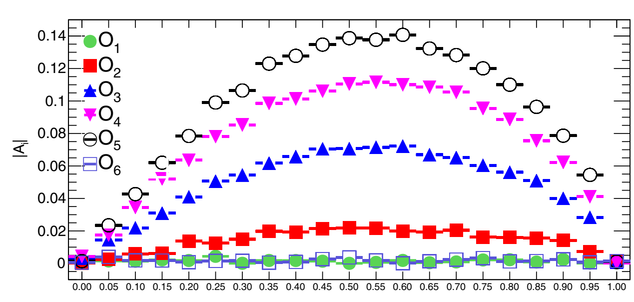


FIG. 3 (color online). Asymmetries generated for observables $O_i$.

Knowing the distribution of asymmetries for given $\tilde{K}_{\mathrm{AZZ}}$ it is possible to obtain the corresponding distributions for any $\tilde{K}_{\mathrm{AZZ}}$ by using the condition $p = \mathrm{const}$.

It is noted, that for the physics model used in this study, the observables $O_1$ and $O_6$ do not generate asymmetries visible with the current Monte Carlo sample. The consistency of these asymmetries with zero confirms that additional effects that are taken into account in our work such as lepton interference, off-shell $ZZ$ production, $ZZ$ background, experimental cuts and detector acceptance do not produce an artificial asymmetry not related with the presence of $CP$-odd terms.The asymmetric behavior is clearly visible for $O_2$ through $O_5$. The asymmetries for $O_4$ and $O_5$ calculated using Eq. (4) may exceed 10% .

In Fig. 3 asymmetry plots are given for $\cos\alpha$ in the range from 0 to 1. For negative $\cos\alpha$ the asymmetries change sign but keep the same shape. This property allows using the asymmetry approach to measure the relative phase in the amplitude of Eq. (2).

The significance of the expected asymmetry can be estimated as

$$S = \Delta N/\sqrt{N} = A_i N_S/\sqrt{N},$$

where $N = N_S + N_B$ is the total number of signal and background events and $\Delta N$ is the difference in the number of events with $O_i < 0$ and $O_i > 0$. It is also noted that $\Delta N \approx \Delta N_S$, because the $ZZ$ background does not contribute to asymmetries at leading order. Following the results of the simulation presented in [43], the number of signal and background events at $\sqrt{s} = 14$ TeV can be estimated as: $N_S = 1.32L$ and $N_B = 0.71L$, respectively. Here $L$ represents the integrated luminosity in $\mathrm{fb}^{-1}$. A data set with the integrated luminosity of 300 $\mathrm{fb}^{-1}$ is expected to be collected during the Run III of the LHC.

Using the above expressions, one can estimate an expected asymmetry of about 9.5% to be measured with this data sample. The corresponding significance will be around two standard deviations. The region $0.340 < \cos\alpha < 0.789$ will then be excluded at 95% C.L.

This exclusion range can be expressed in terms of $f_{g_4}$ fraction of events [4] arising from the anomalous coupling $g_4$,

$$f_{g_4} = \frac{\sigma_4 |g_4|^2}{\sigma_1 |g_1|^2 + \sigma_4 |g_4|^2}, \tag{5}$$

where $g_i$ are couplings of the decay vertex, and $\sigma_i$ is the cross section of the processes $H \to ZZ \to 4l$ corresponding to $g_i = 1, g_{i\neq j} = 0$. Eq. (5) can be rewritten in terms of the mixing angle $\alpha$ as

$$f_{g_4} = \frac{1}{1 + \frac{\sigma_1}{\sigma_4}\left(\frac{k_{\mathrm{SM}}}{\tilde{K}_{\mathrm{AZZ}}}\right)^2 \cot^2\alpha},$$

where the ratio of cross sections $\sigma_4/\sigma_1 = 0.139$ is obtained from the Monte Carlo generator.

The range of the fraction of events of Eq. (5) close to 1 has been already excluded by CMS [4]. Taking this into account, the exclusion limit obtained in the presented analysis becomes $f_{g_4} < 0.207$ at 300 $\mathrm{fb}^{-1}$ for the model

TABLE V. Upper limit on $f_{g_4}$ and $\cos\alpha$ range excluded at the 95% C.L.

| $L$, $\mathrm{fb}^{-1}$ | 300 | | 3000 | |
|---|---|---|---|---|
| $\tilde{K}_{\mathrm{AZZ}}/1.76$ | $\Delta c_\alpha$ | $f_{g_4}$ | $\Delta c_\alpha$ | $f_{g_4}$ |
| 0.6 | ⋯ | ⋯ | 0.122–0.921 | 0.026 |
| 0.8 | 0.431–0.650 | 0.274 | 0.100–0.953 | 0.027 |
| 1.0 | 0.340–0.789 | 0.207 | 0.089–0.968 | 0.028 |
| 1.2 | 0.307–0.852 | 0.191 | 0.087–0.975 | 0.031 |
| 1.4 | 0.297–0.886 | 0.188 | 0.086–0.981 | 0.032 |

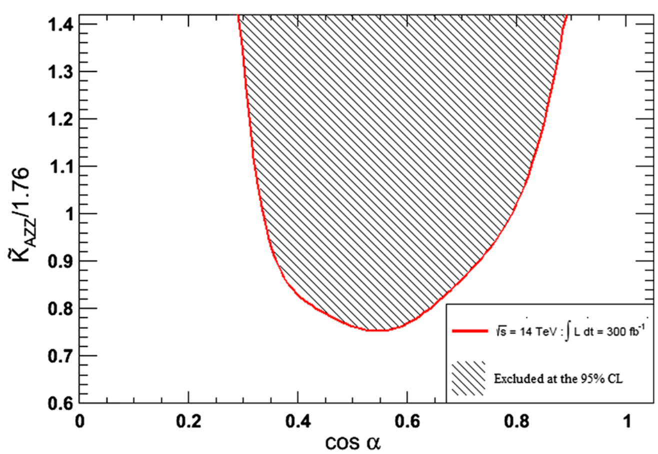


FIG. 4 (color online). The 95% C.L. exclusion limits for model parameters $c_\alpha$, $\tilde{K}_{\mathrm{AZZ}}$ at 300 $\mathrm{fb}^{-1}$. Regions of rejected model parameters are shown.

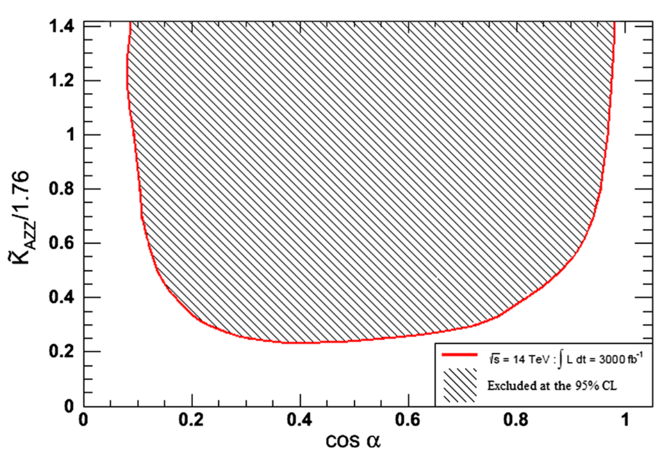


FIG. 5 (color online). The 95% C.L. exclusion limits for model parameters $c_\alpha$, $\tilde{K}_{\mathrm{AZZ}}$ at 3000 $\mathrm{fb}^{-1}$. Regions of rejected model parameters are shown.

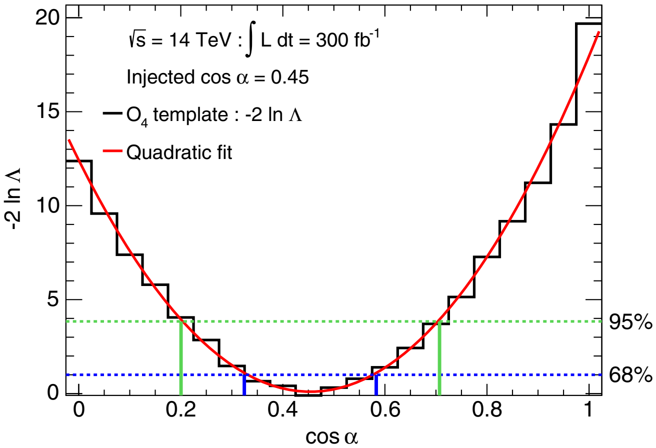


FIG. 6 (color online). Example of the likelihood curve for the mixing angle observable fit of $O_4$. The definitions of the 64% C.L. and 95% C.L. exclusion regions are demonstrated.

described by the Lagrangian of Eq. (3) and parameters given in Table III.

For the high luminosity LHC, assuming the same signal and background yields per fb as above, the following exclusion range can be established: $0.089 < \cos\alpha < 0.968$ at 95% C.L. This corresponds to an upper limit $f_{g_4} = 0.028$ at 3000 fb$^{-1}$.

In the same way as above, we performed estimates for four more values of the model parameter $\tilde{K}_{\mathrm{AZZ}}$. Monte Carlo samples were generated for each point of two dimensional model space $(\cos\alpha, \tilde{K}_{AZZ})$. The number of signal events was calculated as $N_S = N_S^{\mathrm{SM}}\sigma/\sigma^{\mathrm{SM}}$ assuming constant K factors. The results are presented in Table V. These limits on $f_{g_4}$ are close to the ones expected in ATLAS [43] and CMS [4] experiments.

The region of $\tilde{K}_{\mathrm{AZZ}}/1.76$ above 1.4 is not considered. In this region the cross sections exceed the SM cross section by more than a factor of two.

In Figs. 4 and 5 the regions of model parameter space $(c_\alpha, \tilde{K}_{\mathrm{AZZ}})$ excluded by the current analysis are shown. The shadowed areas are excluded at the 95% C.L. Lines in Figs. 4 and 5 represent a polynomial fit to the results of the method of asymmetries.

Note that $CP$-odd observables were studied also in [44]. According to this article the detection of $CP$-violating effects is out of reach of the LHC. However, as was mentioned in [44], these effects might in principle attain large values because of numerical enhancements.

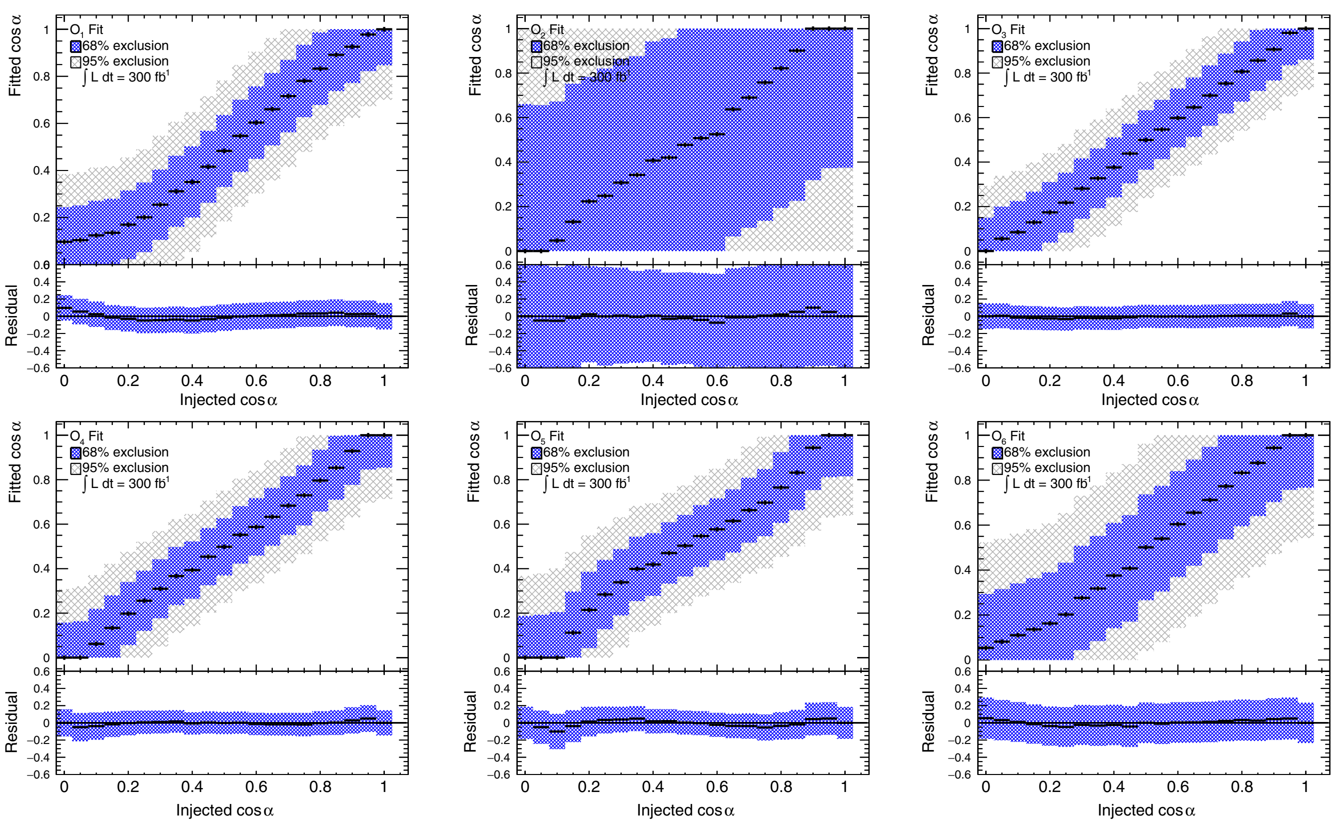


FIG. 7 (color online). Results of the mixing angle $\alpha$ scan produced with the mixing angle observable fit corresponding to the integrated luminosity of 300 fb$^{-1}$.

TABLE VI. Upper limit on $f_{g_4}$ and $\cos\alpha$ range excluded at the 95% C.L. with the mixing angle observable fit. The Standard Model signal is assumed. The BSM templates are generated according to the model defined in Table III with $\tilde{K}_{AZZ} = 1.76$.

| $L$, fb$^{-1}$ | 300 | | 3000 | |
| --- | --- | --- | --- | --- |
| Observable | $\Delta c_\alpha$ | $f_{g_4}$ | $\Delta c_\alpha$ | $f_{g_4}$ |
| $O_1$ | 0–0.695 | 0.315 | 0–0.903 | 0.089 |
| $O_2$ | ... | ... | 0–0.604 | 0.428 |
| $O_3$ | 0–0.719 | 0.287 | 0–0.911 | 0.081 |
| $O_4$ | 0–0.708 | 0.300 | 0–0.908 | 0.084 |
| $O_5$ | 0–0.631 | 0.394 | 0–0.883 | 0.108 |
| $O_6$ | 0–0.533 | 0.520 | 0–0.852 | 0.104 |

## V. MIXING ANGLE OBSERVABLE FIT

The asymmetries $A_i$ discussed in the Sec. IV are integrated quantities of angular observables $O_i$ and, thus, provide limited information about the anomalous contributions to the $HZZ$ vertex. The optimal sensitivity to these contributions can be obtained by studying the shapes of distributions of observables $O_i$ and their correlations.

The sensitivity of individual observables to the presence of anomalous contributions to the $HZZ$ vertex is studied by fitting the shape of these observables as a function of the mixing angle. The likelihood function of the fit is defined as

$$\mathcal{L}(\cos\alpha,\mu,\theta) = \prod_j^{N_{\rm chan}}\prod_i^{N_{\rm bin}} P(N_{i,j}|\mu_j\cdot S_{i,j}(\cos\alpha,\theta)+B_{i,j}(\theta)).$$

Here, besides the parameter of interest $\cos\alpha$, two nuisance parameters have been introduced: the best-fitting signal strength $\mu$ and a systematic normalization uncertainty $\theta$. The likelihood function is a product over the different final states and bins of the specific observable that is being fitted. In each bin, the observed number of events from pseudodata $N$, is compared to the expected number of events of the model $S+B$ assuming a Poissonian distribution of entries $P$. By varying the mixing parameter $\cos\alpha$ of the likelihood for a given data set we can construct the standard log-likelihood test statistic,

$$-2\ln\Lambda(\cos\alpha) = -2\ln\frac{\mathcal{L}(\cos\alpha)}{\mathcal{L}(\cos\hat{\alpha})},$$

where $\hat{\alpha}$ denotes the mixing angle that maximizes the likelihood function over the scan. The other likelihood parameters are profiled at the corresponding $\cos\alpha$ value.

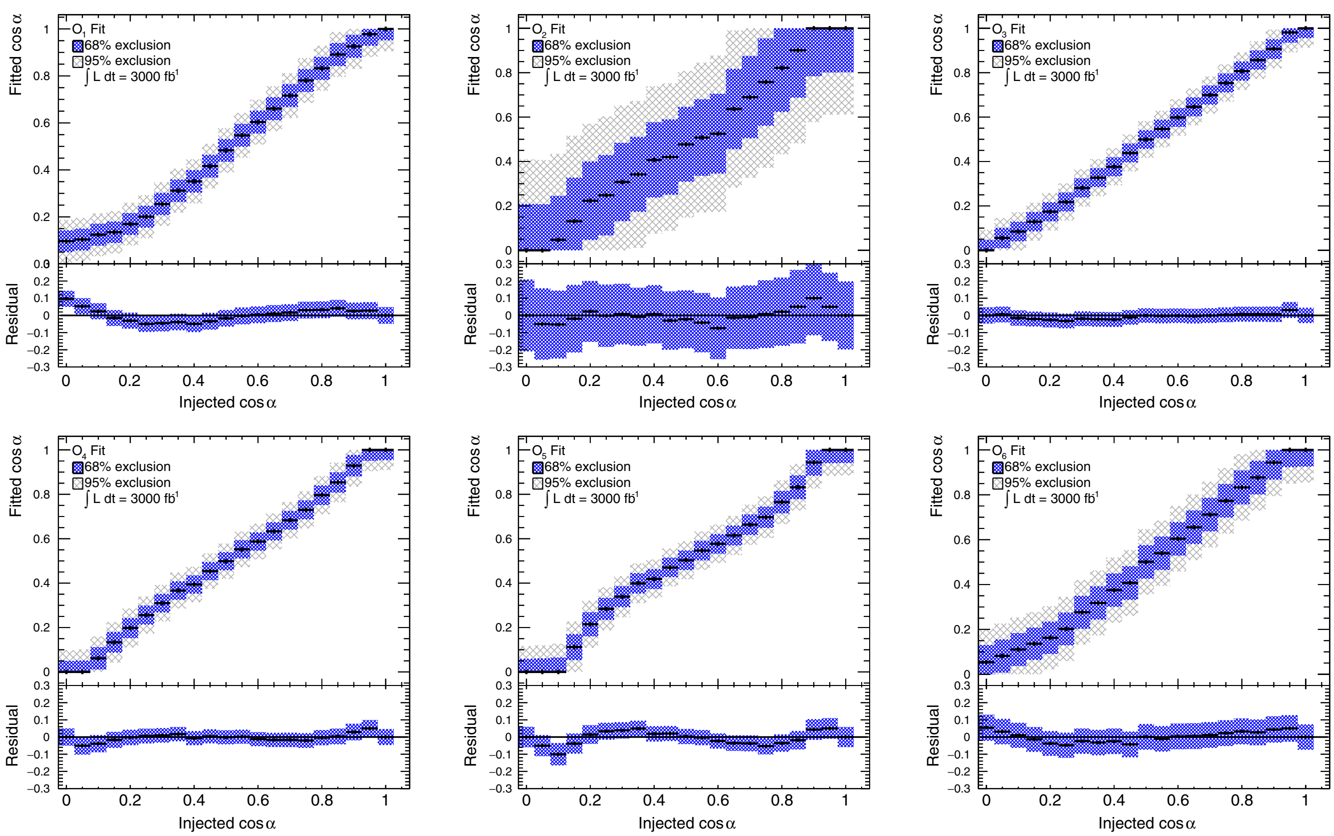


FIG. 8 (color online). Results of the mixing angle $\alpha$ scan produced with the mixing angle observable fit corresponding to the integrated luminosity of 3000 fb$^{-1}$.

The 95% exclusion is reached when $-2\ln\Lambda(\cos\alpha) > 3.84$. The definitions of the 64% C.L. and 95% C.L. exclusion regions are demonstrated in Fig. 6.

Results of the scan of the mixing angle $\alpha$ produced with the mixing angle observable fit corresponding to the integrated luminosity of 300 $\mathrm{fb}^{-1}$ are presented in Fig. 7. The results are reported for the model with $\tilde{K}_{\mathrm{AZZ}} = 1.76$ and remaining parameters as defined in Table III. The values of the mixing angle $\cos\alpha$ used to generate the input pseudodata are marked on the $x$ axis. Every bin of the injected $\cos\alpha$ on represents the null-hypothesis likelihood curve similar to Fig. 6. The $y$ axis shows the $\cos\hat{\alpha}$ values reconstructed in the fit. The dark (blue) and grey dashed areas represent the 64% C.L. and 95% C.L. limits, respectively. The white area in each bin of injected $\cos\alpha$ is excluded at 95% C.L. As expected, the sensitivity to the mixing angle varies for different observables, resulting in significantly different exclusion regions. The weakest exclusion is reached with the $O_2$, while the strongest is reached with the $O_4$.

The results corresponding to the integrated luminosity of 3000 $\mathrm{fb}^{-1}$ are presented in Fig. 8. Compared to 300 $\mathrm{fb}^{-1}$, the 95% C.L. exclusion regions around the fitted $\cos\hat{\alpha}$ values are significantly reduced. Assuming the pure Standard Model signal, the following exclusion limits can be set using the $O_4$ observable alone: $0 < \cos\hat{\alpha} < 0.708$ at the 95% C.L. for 300 $\mathrm{fb}^{-1}$ and $0 < \cos\hat{\alpha} < 0.908$ at the 95% C.L. for 3000 $\mathrm{fb}^{-1}$. The exclusion limits obtained from other observables assuming the Standard Model signal are reported in Table VI.

The exclusion limits obtained for hypothetical BSM signals can be read from Fig. 7 and 8. It is noted that by fitting the shape of the $O_4$ observable alone, the exclusion limits similar to those reported in Sec. IV can be obtained. Further improvements can be obtained by combining several observables in the same fit.

## VI. CONCLUSION

In this article, studies of tensor structure of the $HZZ$ vertex are presented. The investigation is performed using the $pp \to H \to ZZ \to 4l$ process assuming the gluon fusion production of the spin-0 resonance. The background contributions, detector resolution, trigger and selection efficiencies expected for the LHC are taken into account. Two different approaches to detect $CP$-violation effects in the $HZZ$ vertex were used. The first approach is based on a simple counting experiment for angular asymmetries of $CP$-sensitive observables. It was shown that the presence of $CP$ violating terms may result in angular asymmetries exceeding 10%. The 95% C.L. exclusion ranges for the mixing angle at different parameters of spin-0 Higgs boson model including the Standard Model $CP$-even term and anomalous $CP$-odd term $g_4$ are calculated. These results are also presented in terms of the effective cross section fraction $f_{g_4}$. The obtained limits are comparable with the ATLAS and CMS projections for Run III at the LHC and the high-luminosity LHC presented in [4,43].

The sensitivity of individual observables to the presence of anomalous contributions to the $HZZ$ vertex was studied by fitting the shape of these observables as a function of the mixing angle. It is demonstrated that using a single most sensitive observable, this approach gives $f_{g_4}$ limits comparable with asymmetries method and with the ATLAS and CMS projections. Compared to the method of angular asymmetries, this approach has an advantage of using the complete shape information of $CP$-odd observables. It is demonstrated that some of the observables, that do not generate significant angular asymmetry in presence of significant $CP$-mixing, can still provide restrictive $f_{g_4}$ limits when their complete shape is analyzed. Combining several $CP$-odd observables in the same fit or combining several angular asymmetries would likely further improve sensitivity to the $CP$ violating coupling. It is noted that careful experimental investigation of all observables, even not the leading ones, is important, since they probe different terms of the $HZZ$ vertex.

## ACKNOWLEDGMENTS

We would like to thank our ATLAS and CMS colleagues for many fruitful discussions and suggestions. We also thank MadGraph and JHU teams for much useful advice. We are grateful to A. Mincer for reading the manuscript and providing valuable suggestions. We thank A. Baumgartner, D. Gray, and T. Reid for their help with the MC samples production. The work of R. Konoplich is partially supported by the U.S. National Science Foundation under Grants No. PHY-1205376 and No. PHY-1402964. The work of K. Prokofiev is partially supported by a grant from the Research Grants Council of the Hong Kong Special Administrative Region, China (Project No. CUHK4/CRF/13G).

[1] CMS Collaborations, Phys. Lett. B **716**, 30 (2012).
[2] ATLAS Collaborations, Phys. Lett. B **716**, 1 (2012).
[3] ATLAS Collaborations, Phys. Lett. B **726**, 88 (2013).
[4] CMS Collaboration, arXiv:1411.3441.
[5] CMS Collaboration, Phys. Rev. Lett. **110**, 081803 (2013).
[6] ATLAS Collaborations, Phys. Lett. B **726**, 120 (2013).
[7] D. Chang, W.-Y. Keung, and I. Phillips, Phys. Rev. D **48**, 3225 (1993).

[8] B. Grzadkowski and J. Gunion, Phys. Lett. B **350**, 218 (1995).

[9] J. F. Gunion, B. Grzadkowski, and X.-G. He, Phys. Rev. Lett. **77**, 5172 (1996).

[10] B. Grzadkowski, J. F. Gunion, and J. Kalinowski, Phys. Rev. D **60**, 075011 (1999).

[11] B. Grzadkowski, J. F. Gunion, and J. Pliszka, Nucl. Phys. **B583**, 49 (2000).

[12] T. Plehn, D. L. Rainwater, and D. Zeppenfeld, Phys. Rev. Lett. **88**, 051801 (2002).

[13] S. Choi, D. Miller, M. Muhlleitner, and P. Zerwas, Phys. Lett. B **553**, 61 (2003).

[14] C. Buszello, I. Fleck, P. Marquard, and J. van der Bij, Eur. Phys. J. C **32**, 209 (2004).

[15] V. Hankele, G. Klamke, D. Zeppenfeld, and T. Figy, Phys. Rev. D **74**, 095001 (2006).

[16] R. M. Godbole, D. Miller, and M. M. Muhlleitner, J. High Energy Phys. 12 (2007) 031.

[17] W.-Y. Keung, I. Low, and J. Shu, Phys. Rev. Lett. **101**, 091802 (2008).

[18] S. Berge and W. Bernreuther, Phys. Lett. B **671**, 470 (2009).

[19] Q.-H. Cao, C. B. Jackson, W.-Y. Keung, I. Low, and J. Shu, Phys. Rev. D **81**, 015010 (2010).

[20] A. De Rujula, J. Lykken, M. Pierini, C. Rogan, and M. Spiropulu, Phys. Rev. D **82**, 013003 (2010).

[21] Y. Gao, A. V. Gritsan, Z. Guo, K. Melnikov, M. Schulze, and N. V. Tran, Phys. Rev. D **81**, 075022 (2010).

[22] S. Berge, W. Bernreuther, B. Niepelt, and H. Spiesberger, Phys. Rev. D **84**, 116003 (2011).

[23] F. Bishara, Y. Grossman, R. Harnik, D. J. Robinson, J. Shu, and J. Zupan, J. High Energy Phys. 04 (2014) 084.

[24] R. Harnik, A. Martin, T. Okui, R. Primulando, and F. Yu, Phys. Rev. D **88**, 076009 (2013).

[25] S. Berge, W. Bernreuther, and H. Spiesberger, Phys. Lett. B **727**, 488 (2013).

[26] A. Menon, T. Modak, D. Sahoo, R. Sinha, and H. Y. Cheng, Phys. Rev. D **89**, 095021 (2014).

[27] Y. Chen, R. Harnik, and R. Vega-Morales, Phys. Rev. Lett. **113**, 191801 (2014).

[28] J. S. Gainer, J. Lykken, K. T. Matchev, S. Mrenna, and M. Park, Phys. Rev. Lett. **111**, 041801 (2013).

[29] P. Avery *et al.*, Phys. Rev. D **87**, 055006 (2013).

[30] J. S. Gainer, J. Lykken, K. T. Matchev, S. Mrenna, and M. Park, Phys. Rev. D **91**, 035011 (2015).

[31] M. Chen, T. Cheng, J. S. Gainer, A. Korytov, K. T. Matchev, P. Milenovic, G. Mitselmakher, M. Park, A. Rinkevicius, and M. Snowball, Phys. Rev. D **89**, 034002 (2014).

[32] D. Stolarski and R. Vega-Morales, Phys. Rev. D **86**, 117504 (2012).

[33] W. Buchmüller and D. Wyler, Nucl. Phys. **B268**, 621 (1986).

[34] B. Grzadkowski, M. Iskrzynski, M. Misiak, and J. Rosiek, J. High Energy Phys. 10 (2010) 085.

[35] S. Bolognesi, Y. Gao, A. V. Gritsan, K. Melnikov, M. Schulze, N. V. Tran, and A. Whitbeck, Phys. Rev. D **86**, 095031 (2012).

[36] I. Anderson *et al.*, Phys. Rev. D **89**, 035007 (2014).

[37] J. Alwall, M. Herquet, F. Maltoni, O. Mattelaer, and T. Stelzer, J. High Energy Phys. 06 (2011) 128.

[38] P. Artoisenet *et al.*, J. High Energy Phys. 11 (2013) 043.

[39] I. Anderson *et al.*, 2014, http://www.pha.jhu.edu/spin/manJHUGenerator.v4.8.1.pdf.

[40] T. Sjostrand, S. Mrenna, and P. Z. Skands, J. High Energy Phys. 05 (2006) 026.

[41] ATLAS Collaboration, J. Instrum. **3**, S08003 (2008).

[42] CMS Collaboration, J. Instrum. **3**, S08004 (2008).

[43] ATLAS Collaboration, Report No. ATL-PHYS-PUB-2013-013, 2013.

[44] G. Buchalla, O. Cata, and G. D'Ambrosio, Eur. Phys. J. C **74**, 2798 (2014).